

AD-A229 971

TTTB FILE COPY

2

RADC-TR-90-280
Final Technical Report
November 1990

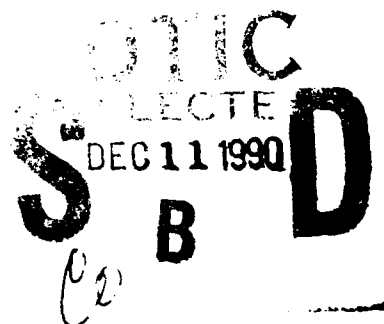


DEVELOPMENT OF OPTICAL FIBERS WITH EMBEDDED GRATINGS FOR SENSOR AND SIGNAL PROCESSING APPLICATIONS

United Technologies Research Center

This effort was funded totally by the Laboratory Director's Fund

Approved for public release; distribution unlimited.

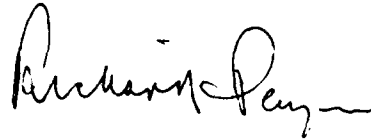


ROME AIR DEVELOPMENT CENTER
Air Force Systems Command
Griffiss Air Force Base, NY 13441-5700

This report has been reviewed by the RADC Public Affairs Division (PA) and is releasable to the National Technical Information Service (NTIS). At NTIS it will be releasable to the general public, including foreign nations.

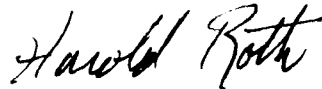
RADC-TR-90-280 has been reviewed and is approved for publication.

APPROVED:



RICHARD PAYNE
Project Engineer

APPROVED:



HAROLD ROTH
Director of Solid State Sciences

FOR THE COMMANDER:



IGOR G. PLONISCH
Directorate of Plans & Programs

If your address has changed or if you wish to be removed from the RADC mailing list, or if the addressee is no longer employed by your organization, please notify RADC (ESO) Hanscom AFB MA 01731-5000. This will assist us in maintaining a current mailing list.

Do not return copies of this report unless contractual obligations or notices on a specific document require that it be returned.

REPORT DOCUMENTATION PAGE

Form Approved
OMB No. 0704-0188

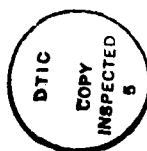
Public reporting burden for this collection of information is estimated to average 1 hour per response, including the time for reviewing instructions, searching existing data sources, gathering and maintaining the data needed, and completing and reviewing the collection of information. Send comments regarding this burden estimate or any other aspect of this collection of information, including suggestions for reducing this burden, to Washington Headquarters Services, Directorate for Information Operations and Reports, 1215 Jefferson Davis Highway, Suite 1204, Arlington, VA 22202-4302, and to the Office of Management and Budget, Paperwork Reduction Project (0704-0188), Washington, DC 20503.

1. AGENCY USE ONLY (Leave Blank)		2. REPORT DATE November 1990		3. REPORT TYPE AND DATES COVERED Final Dec 87 - Dec 89	
4. TITLE AND SUBTITLE DEVELOPMENT OF OPTICAL FIBERS WITH EMBEDDED GRATINGS FOR SENSOR AND SIGNAL PROCESSING APPLICATIONS				5. FUNDING NUMBERS C - F19628-88-C-0033 PE - 61101F PR - LDFP TA - 05 WU - C8	
6. AUTHOR(S) W. W. Morey, W. H. Glenn, G. Meltz					
7. PERFORMING ORGANIZATION NAME(S) AND ADDRESS(ES) United Technologies Research Center 400 Main Street E. Hartford CT 06108				8. PERFORMING ORGANIZATION REPORT NUMBER	
9. SPONSORING/MONITORING AGENCY NAME(S) AND ADDRESS(ES) Rome Air Development Center (ESO) Hanscom AFB MA 01731-5000				10. SPONSORING/MONITORING AGENCY REPORT NUMBER RADC-TR-90-280	
11. SUPPLEMENTARY NOTES RADC Project Engineer: Richard Payne/ESO/(617) 377-5129 This effort was funded totally by the Laboratory Director's Fund.					
12a. DISTRIBUTION/AVAILABILITY STATEMENT Approved for public release; distribution unlimited.				12b. DISTRIBUTION CODE	
13. ABSTRACT (Maximum 200 words) Bragg gratings have been fabricated in the core of germanium-doped silica optical fibers using a photorefractive property of the glass. The process depends on an oxygen vacancy defect in the germania-silica core manifested by a strong absorption peak occurring in the uv at 245 nm. The absorption can be bleached by irradiation at the absorbing wavelength leaving behind a residual small refractive index change. By irradiation with a holographic interference pattern, a phase grating of controlled periodicity is introduced into the fiber core. This report describes the grating fabrication technique and experimental work defining the optical characteristics of the grating and application to practical devices.					
14. SUBJECT TERMS Bragg grating, Fiber optic sensors, Embedded fiber grating, Strain sensors, Signal processing elements, Laser Bragg reflectors.				15. NUMBER OF PAGES 44	
				16. PRICE CODE	
17. SECURITY CLASSIFICATION OF REPORT UNCLASSIFIED	18. SECURITY CLASSIFICATION OF THIS PAGE UNCLASSIFIED	19. SECURITY CLASSIFICATION OF ABSTRACT UNCLASSIFIED	20. LIMITATION OF ABSTRACT UL		

Development of Optical Fibers with Embedded Gratings for Sensor and Signal Processing Applications

TABLE OF CONTENTS

	<u>Page</u>
1.0 INTRODUCTION AND SUMMARY	1
2.0 BRAGG GRATINGS IN OPTICAL FIBERS	4
2.1 Phenomenological Model Of The Photorefractive Effect	4
2.2 Basic Properties of Bragg Gratings	8
2.3 Production of Bragg Gratings	11
2.4 Mode and Polarization Dependence of Reflectivity	17
2.5 Temperature And Strain Sensitivity	20
2.6 Coupling of radiation Out of a Fiber by a Grating	22
2.7 Locking and Tuning of an External Cavity Semiconductor Laser with an Embedded Fiber Grating Reflector	25
2.8 Multiple Grating Configurations	27
3.0 CONCLUSIONS	30
4.0 REFERENCES	32
5.0 PUBLICATIONS AND PRESENTATIONS	33



Accession For	
NTIS SPA&I	<input checked="" type="checkbox"/>
DTIC TAB	<input type="checkbox"/>
Unannounced	<input type="checkbox"/>
Justification	
By	
Distribution/	
Availability Codes	
Normal and/or	
Dist	Special
A-1	

1.0 INTRODUCTION AND SUMMARY

This report summarizes the work carried out under Contract F19628-88-C0033, Development of Optical Fibers with Embedded Gratings for Signal Processing and Sensor Applications. The program involved work with photorefractively formed Bragg gratings in the core of optical fibers. A Bragg grating is a periodic variation in the index of refraction of the fiber core. Such a structure can have a strong and wavelength selective reflectivity peak for radiation propagating in the core. The peak occurs when the wavelength of the radiation is twice the period of the grating. This is known as the Bragg condition; it is the condition for which radiation scattered from all parts of the grating adds up coherently in the backward direction.

Work on this program has demonstrated that it is possible to produce strong Bragg reflectors in a variety of fibers using transverse UV illumination. This has important implications for a variety of sensor and signal processing applications. The technique allows the production of narrowband reflectors of easily controllable reflectivity, center frequency and bandwidth at any desired point or points in an optical fiber system. This will allow implementation of a variety of novel optical elements including narrowband transmission and reflection filters, wavelength selective couplers, filters with complex and controllable transmission characteristics, wavelength multiplexing elements and distributed sensor systems.

Photorefractive formation of Bragg gratings in germanosilicate fibers was first observed by Hill et al. [1] in 1978. In these experiments, a standing wave interference pattern from counterpropagating beams of green radiation from an argon ion laser gave rise to a permanent change in the index of refraction in the fiber core. The periodicity of the index change was identical to the periodicity of the intensity in the interference pattern. It was also observed that the strength of the index change was proportional to the square of the intensity of the exposing radiation, suggesting that a two photon process was involved.

This latter observation suggested to workers at UTRC that it might be possible to form grating more efficiently by a one photon process using ultraviolet radiation. Some initial experiments were carried out. It was found that germania and germanosilicate glasses have an absorption peak at

245 nm. This peak may be bleached by exposure to UV radiation. It is hypothesized that the bleaching of this absorption, coupled possibly with the formation of other absorption peaks is responsible for the photorefractive index change. Prior to the start of the program, some initial experiments were carried out using a doubled argon laser. It was shown that gratings could be produced by transverse illumination, and some relatively weak gratings were fabricated.

Under this program, the major accomplishments were:

- Use of a higher power UV source to generate strong gratings in the visible and near infrared regions of the spectrum. The gratings were produced by transverse illumination and were localized.
- Demonstration of the strain sensitivity of the grating
- Demonstration of the temperature sensitivity of the gratings.
- Demonstration of the persistence of the gratings at temperatures up to 500°C.
- Demonstration of the dependence of the reflectivity on the transverse modes of the fiber.
- Fabrication of gratings in polarization preserving fiber and demonstration of the polarization dependence of the reflectivity.
- Analysis and demonstration of outcoupling of radiation from normal and tilted gratings in isotropic and in polarization preserving fibers.
- Use of a Bragg grating in an external cavity semiconductor to achieve single mode operations.
- Demonstration of the tuning of an external cavity semiconductor laser by strain-tuning of the Bragg reflector.
- Analysis of the characteristics of configurations involving multiple, spaced gratings.

The major part of the experimental work on this program was carried out by W. W. Morey with the technical assistance of A. W. Wilson. Analytical support was provided by W. H. Glenn and G. Meltz. C. M. Ferrar carried out the experiments involving the semiconductor laser.

2.0 BRAGG GRATINGS IN OPTICAL FIBERS

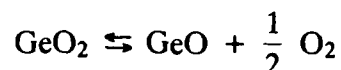
2.1 PHENOMENOLOGICAL MODEL OF THE PHOTOREFRACTIVE EFFECT

The formation of Bragg gratings in optical fibers was first observed by K. O. Hill et al. [1] in 1978. In these early experiments, it was observed that if radiation from a 488 nm argon laser was injected into a single mode, germania doped fiber, the reflectivity of the fiber grew from its initially low Fresnel value ($\sim 4\%$) to a value which could be over 90%. The explanation proposed for this observation was that a weak standing wave which was initially present in the fiber due to the Fresnel reflection initiated the formation of a grating. As the grating formed, the intensity of the backward propagating wave increased, leading to the formation of a stronger grating. This bootstrap process continued until the reflectivity saturated at a relatively high value. The narrow linewidth was confirmed by tuning the grating line through the laser line by stretching the fiber. In other experiments gratings were formed starting with two initially counterpropagating waves in the fiber.

The intensity of the radiation used in these experiments was quite high, approximately .5 watts in a single mode fiber. It was observed that the strength of the grating produced was proportional to the square of the writing power. It was also observed that different fibers with nominally the same concentration of germania did not exhibit the same degree of photorefractivity, some in fact showing no effect.

The potential utility of embedded gratings for sensor and signal processing applications was recognized by workers at UTRC, and a program was initiated to explore the phenomenon. The quadratic dependence of the grating strength on the writing power and the high optical intensities suggested that a two photon process was producing the photorefractivity. This led to the question of whether the effect could be produced at a much lower intensity by a one photon process using radiation at one half the wavelength (twice the energy per photon) of that used in the Hill experiments. It was determined from published data and by direct experimental measurement that germania and germania doped silica can have a strong absorption peak at a wavelength of 245 nm, roughly one half the wavelength of the argon line. This absorption is not an intrinsic property of germania; it is believed

to be due to the presence of oxygen vacancy defects in the lattice. The density of these defect depends on the thermal history of the glass and is related to the dissociation reaction



that can occur at elevated temperatures. It has been found by R. Weeks [2] that if the glass is maintained at an elevated ($\sim 1600^\circ\text{C}$) temperature and then allowed to cool rapidly to room temperature, many defects are formed. In the case of the optical fibers the defects could be present in the preform or they could be formed in the drawing process since in drawing the fiber the preform is maintained at high temperature and the glass cools rapidly as the fiber is drawn off. This could explain the variability that is seen in nominally similar fibers.

It has been reported in the literature and confirmed experimentally at UTRC that the UV absorption band can be bleached by exposure to radiation lying within the band. This suggests a model for the photorefractive effect. With any absorption line there is an associated dispersion which makes a contribution to the total index of refraction of the material. The dispersion due to a given line is uniquely related to the absorption line shape by the Kramers-Kronig relation. This is completely independent of the mechanism responsible for the absorption line. If the absorption line is bleached by UV radiation, then its associated dispersion will also be bleached and the refractive index will change. Although the absorption band may be narrow, the dispersion extends far beyond the band and, in fact, remains finite for extremely long wavelengths (all the way to $\lambda = \infty$ or $\omega = 0$). The absorption peak near 245 nm is evident. It is a strong absorption, having an optical density of about 0.7 for a sample thickness of only 41 microns. The figure also shows the bleaching due to exposure to 249 nm radiation from a KrF excimer laser.

This may be put on a more quantitative basis. Using a simple Lorentz oscillator model for the absorption line it is straightforward to show that the propagation vector k is given by

$$k = \frac{2\pi n_0}{\lambda} + \frac{1}{2} \alpha \frac{\Delta\lambda}{\lambda} \frac{\left(1 - \frac{\lambda_0^2}{\lambda^2}\right) + i \frac{\Delta\lambda}{\lambda}}{\left(1 - \frac{\lambda_0^2}{\lambda^2}\right)^2 + \left(\frac{\Delta\lambda}{\lambda}\right)^2}$$

where α is the absorption coefficient at line center, λ_0 is the wavelength of the line center and $\Delta\lambda$ is the line width (FWHM). The absorption coefficient is

$$\alpha(\lambda) = \frac{\alpha \left(\frac{\Delta\lambda}{\lambda}\right)^2}{\left(1 - \frac{\lambda_0^2}{\lambda^2}\right)^2 + \left(\frac{\Delta\lambda}{\lambda}\right)^2} = \alpha \text{ if } \lambda = \lambda_0$$

The change in index is related to the real part of the propagation constant by

$$\Delta n = \frac{\alpha \Delta\lambda}{4\pi} \frac{\left(1 - \lambda_0^2/\lambda^2\right)}{\left(1 - \frac{\lambda_0^2}{\lambda^2}\right)^2 + \left(\frac{\Delta\lambda}{\lambda}\right)^2}$$

Far away from the absorption band (on the long wavelength side), this reduces to

$$\Delta n = \frac{\alpha \Delta\lambda}{4\pi}$$

Figure 2-1 shows an absorption spectrum of a sample of germania glass that was prepared at UTRC. (The composition of this glass was 100% GeO_2 .) The glass was exposed to ultraviolet radiation from a KrF excimer laser as indicated. The 245 nm peak is clearly visible in the unexposed trace and is nearly completely bleached out at the long exposure. The optical density at the peak of approximately 0.7 corresponds to an absorption coefficient of 400/cm. Figure 2-2 shows a plot of the absorption and associated dispersion from the Lorentz model. The measured peak absorption was used in the model

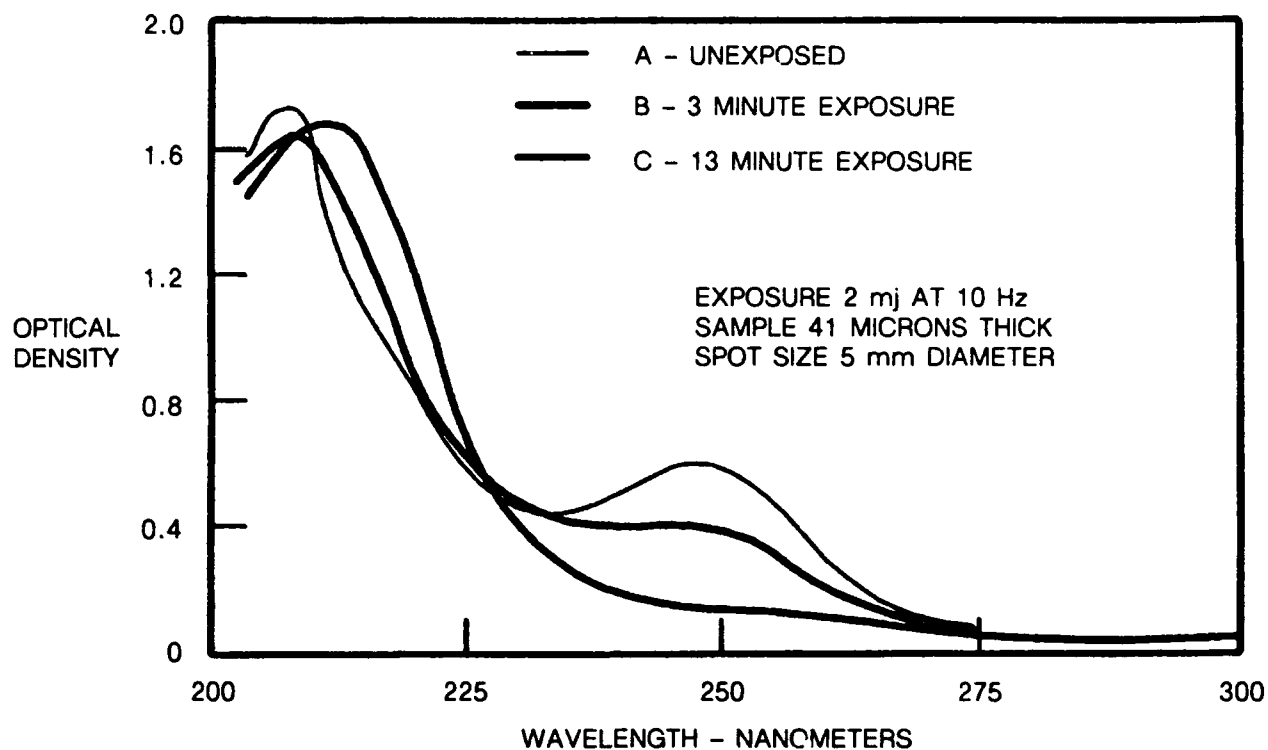


Fig. 2-1. Bleaching of UV absorption in GeO_2 .

89-6-66-2

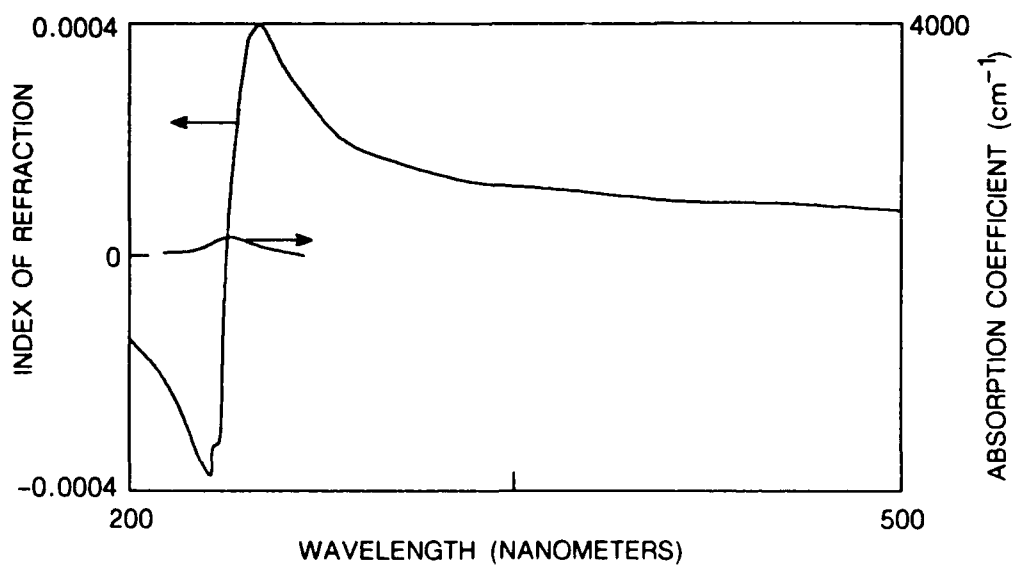


Fig. 2-2. Absorption and dispersion in a fiber.

90-1-49-1

and a linewidth of 20 nm was assumed. In the visible, the index change associated with the absorption line is about 10^{-4} and varies only weakly with wavelength. This is not meant to be a quantitative comparison with the experimental results to be presented, but rather an indication of the order of magnitude of the effects involved.

In this analysis it was not necessary to make explicit use of the Kramers–Kronig relation to derive the real part of the index change from the imaginary part (the absorption). The K–K relation derives from the requirement that the system be causal, i.e., that it does not have an output before the input is applied. The Lorentz model for the index is causal so that the K–K relation is automatically satisfied.

This phenomenological model certainly does not describe all the processes that may be occurring. Additional absorption lines could be produced by the irradiation, possibly in the vacuum ultraviolet region which is not accessible to observation. It does provide confidence, however, that the index changes observed in the visible and near IR should also be present in the 1300 nm and 1500 nm bands.

The ability to produce photorefractive index changes with low power ultraviolet radiation has important implications for the fabrication of practical devices based on Bragg gratings. In the experiments of Hill et al. [1] a high power density was required because of the two photon process. The radiation had to be propagating in the core. Because of this, the grating was produced along the whole length of the fiber. The periodicity of the grating was determined by the wavelength of the exposing radiation. With UV exposure, a transverse illumination, as shown in Fig. 2-3, may be used. This allows localization of the grating in the fiber. The periodicity may also be conveniently changed by changing the angle between the interfering beams.

2.2 BASIC PROPERTIES OF BRAGG GRATINGS

The basic properties of a Bragg grating are indicated schematically in Fig. 2-4. The periodic perturbation of the index in the fiber core is represented by the shading. Each perturbation will scatter a small portion of the incident radiation. Generally, the radiation scattered by the different portions of the grating will be mutually out of phase and will tend to cancel. For one particular condition, namely

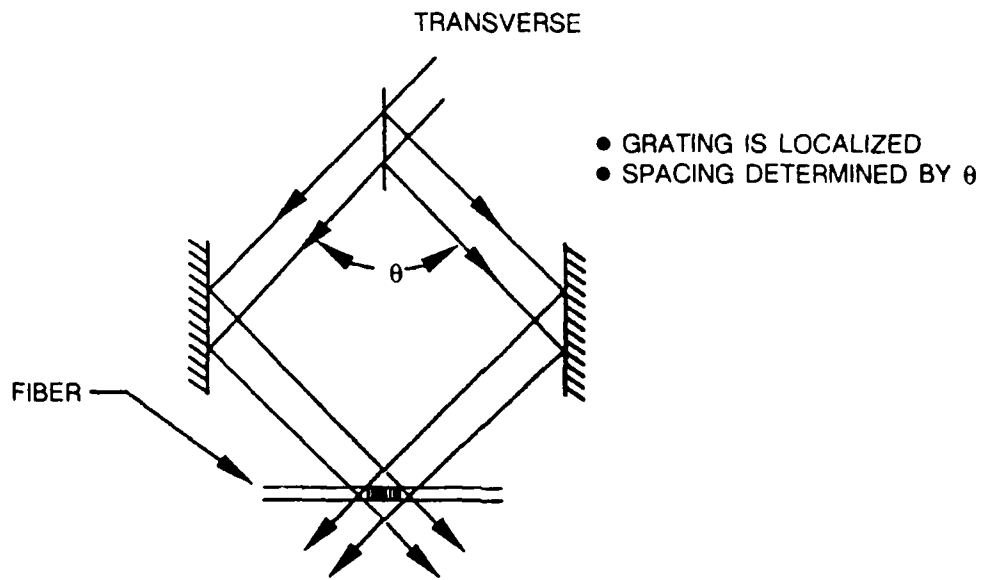
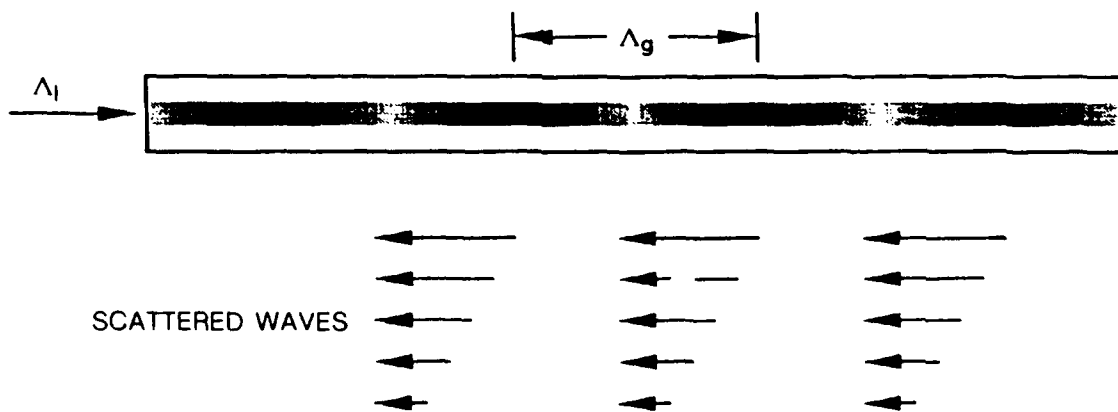


Fig. 2-3. Writing a grating in a fiber.

90-1-49-2



WHEN $\lambda_g = \lambda_i/2$ ALL THE SCATTERED WAVES ARE IN PHASE AND A STRONG REFLECTION OCCURS

Fig. 2-4. Embedded grating in an optical fiber.

90-1-49-3

when the wavelength of the incident radiation is twice the period of the grating, all the contributions will add up coherently in the backward direction, and a reflectivity peak will occur.

Analytical descriptions of the reflection and transmission properties of gratings have been quite thoroughly worked out using coupled mode theory (see, for example, Lam and Garside [3]). The reflectivity is given by

$$R(\lambda_n L) = \frac{\Omega^2 \sinh^2 (SL)}{\Delta k^2 \sinh^2 (SL) + S^2 \cosh^2 (SL)}$$

where

- R = reflectivity
- L = grating length
- Ω = coupling coefficient
- Δk = $k - k_g/2$
- S = $(\Omega^2 - \Delta k^2)^{1/2}$

The coupling coefficient Ω is

$$\Omega = \frac{\pi L}{\lambda} \Delta n \eta$$

where η is the fraction of the fundamental mode propagating in the core. At the line center, the expression for the reflectivity becomes

$$R = \tanh^2 \Omega L$$

If the grating is weak, a simpler expression for the reflectivity may be derived from the Born approximation. The result is

$$R = (\Delta n)^2 \frac{\sin^2 \Delta k L}{(\Delta k L)^2}$$

From this expression it may readily be seen that the width of the peak (full width between the first zeros is

$$\Delta kL = \pm \pi$$

$$n \frac{2\pi \Delta f L}{c} = \pm \pi$$

$$\Delta f_{FW} = \frac{c}{nL}$$

In the above analysis it has been assumed that the phase fronts of the grating (i.e., the surfaces of constant index change) are perpendicular to the core of the fiber. The case where they are tilted is also of considerable interest since it allows coupling of radiation out of the core. This will be discussed in a later section of this report.

2.3 PRODUCTION OF BRAGG GRATINGS

As indicated above, the basic technique for producing a grating involves formation of an interference pattern between two intersecting UV beams and exposing the fiber to the interference pattern. It is necessary to remove the buffer coating from the fiber since most buffer materials are opaque to the ultraviolet radiation.

In early experiments, a high power argon laser (Coherent Inc.) was frequency doubled in a commercial temperature tuned KDP frequency doubler (INRAD) to produce an ultraviolet beam at 514/2 or 488/2 nm. This arrangement produced a beam of about 2 mw average power for an input of 2 watts. When the input power was increased above this level, the quality of the beam deteriorated without significant increase in UV power. This system was used to make some relatively weak gratings, but was abandoned in favor of the arrangement shown in Fig. 2-5. A Lambda Physik XeCl excimer laser operating at 308 nm was used to pump a Lambda Physik tunable dye laser. The dye laser incorporated a grating and an etalon to tune the wavelength and narrow the line. This laser produced an output at about 490 nm. This radiation was then doubled in a BBO (beta barium borate) crystal to produce an ultraviolet beam at 245 nm. This rather elaborate arrangement was needed to ensure adequate coherence in the UV beam. To produce a grating, the coherence length of the interfering

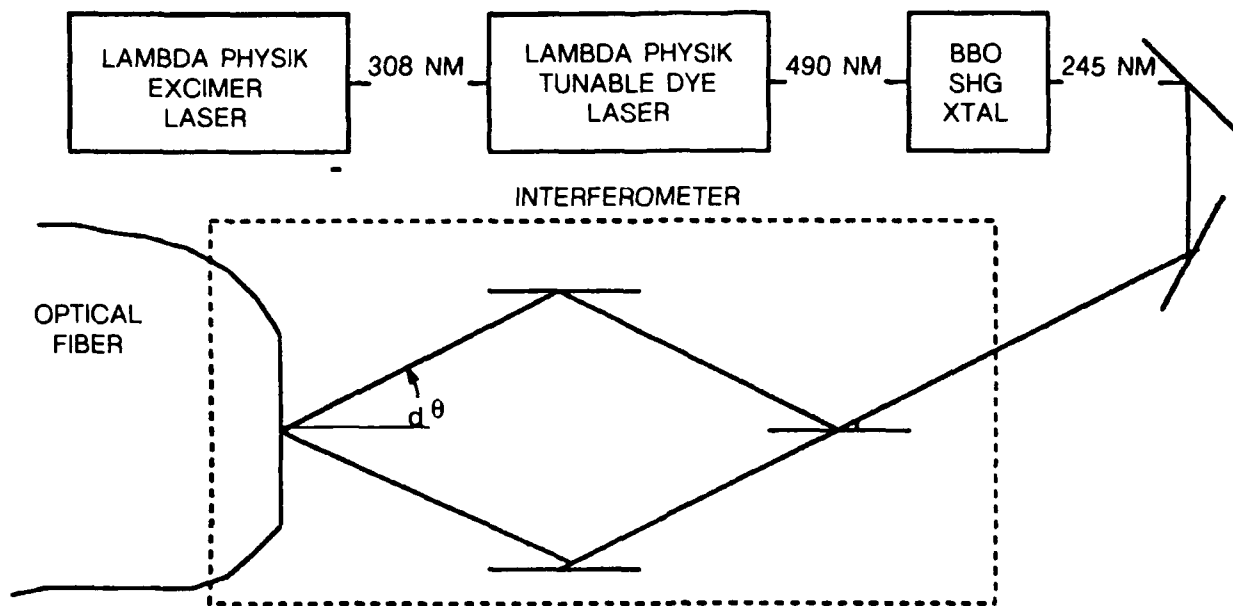


Fig. 2-5. Experimental setup for the production of gratings.

89-6-66-3

beams must be at least as long as the desired grating length. The manufacturer's specifications give a coherence length of 20 cm for the dye laser. When the radiation is doubled, the bandwidth is doubled and the coherence length is reduced by a factor of two to give a 10 cm coherence length. The excimer laser operated in a repetitively pulsed mode producing pulses of 20 ns duration at rates up to 80 Hz.

The UV beam was split and recombined in the interferometer as shown, and the fiber to be exposed was placed at the intersection point of the beams. The periodicity of the grating could be varied by varying the angle of intersection of the beams or by varying the UV wavelength. The period of the grating is given by

$$\lambda_g = \frac{\lambda_w}{2 \sin \theta}$$

λ_w = exposing (writing) wavelength

where θ is the half angle between the intersecting beams. Although the interference pattern is formed in glass, its period is the same as it would be if the beams were interfering in air. This is a result of the refraction of the beams coupled with the shortening of the wavelength as they enter the glass. The wavelength of radiation propagating in the core of the fiber is

$$\lambda_f = \frac{\lambda_r}{n}$$

$$\lambda_r = \text{free space reading wavelength}$$

and the Bragg condition for back reflection is

$$\lambda_f = 2\lambda_g$$

$$\lambda_r = \frac{n\lambda_w}{\sin \theta}$$

A filtered arc lamp and monochromator were used to monitor the transmission of the fiber. A separate setup could be used to monitor the reflectivity of the grating in the fiber. The reflected signal was monitored by placing a beam splitter at the fiber input and comparing the reflected power to the power reflected at a wavelength near but out of the grating band by a mirror at the output end of the fiber.

Gratings were produced in a variety of fibers including a commercial (Spectran) 6.6 mole percent germanosilicate core fiber, a fiber of the type used by Hill et al [1], an elliptical core, polarization maintaining fiber (Andrew Corp.), and a very high germania content custom made fiber (Polaroid Corp.).

Figure 2-6 shows a typical result obtained for a grating at approximately 578 nm. These data were obtained using the Spectran fiber. The FWHM of this grating was 42 GHz. The formula presented earlier predicts a full width between the first zeros of about 45 GHz, so the grating is somewhat wider than predicted by the model. In a separate experiment, the reflectivity of the grating was monitored. The intensity of the reflected signal was monitored with and without a 100% reflector at the far end of

the fiber. The results are also shown in the figure. This confirms that the light lost in transmission is actually reflected and not absorbed or scattered.

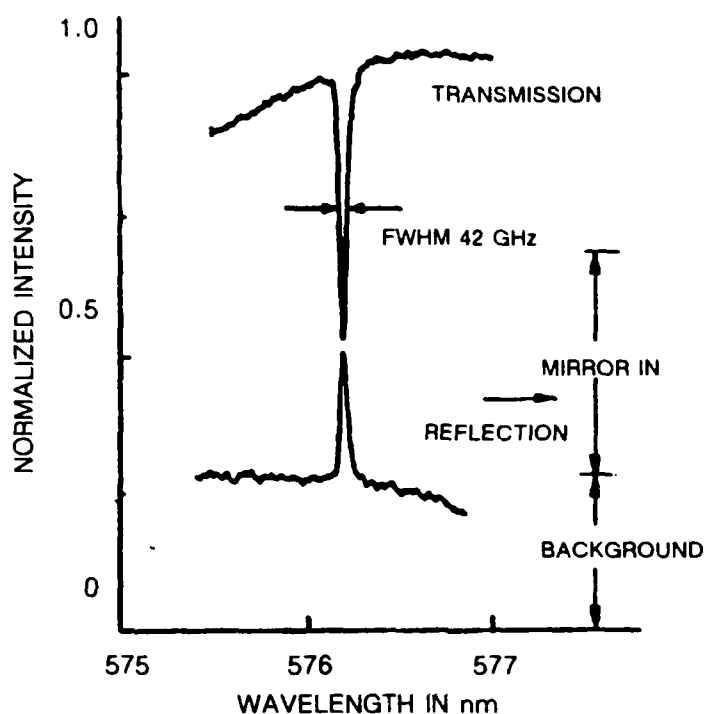


Fig. 2-6. Transmission and reflection spectra for 4.4 mm grating. 89-6-66-4

Gratings were also produced at 820 nm. Figure 2-7 shows the transmission spectrum of such a grating. In this case, the grating was longer, about one centimeter, and the width is reduced accordingly.

The strength of the index perturbation may be estimated from the measured reflectivity and the grating length. Figure 2-8 shows the theoretical prediction of the grating reflectivity as a function of the length and magnitude of the index change. The experimental point at 50% reflectivity corresponds to the 580 nm grating discussed above and the higher reflectivity point corresponds to a grating at 820 nm. The lower reflectivity point is a grating produced earlier using the frequency doubled argon laser. The magnitudes of the index changes are in good agreement with the phenomenological model presented earlier. That model predicted a change of about 10^{-4} , but was based on the measured absorption of a sample of 100% GeO_2 . The germania content of the fiber core is substantially lower so that changes of a few parts in 10^5 are quite reasonable.

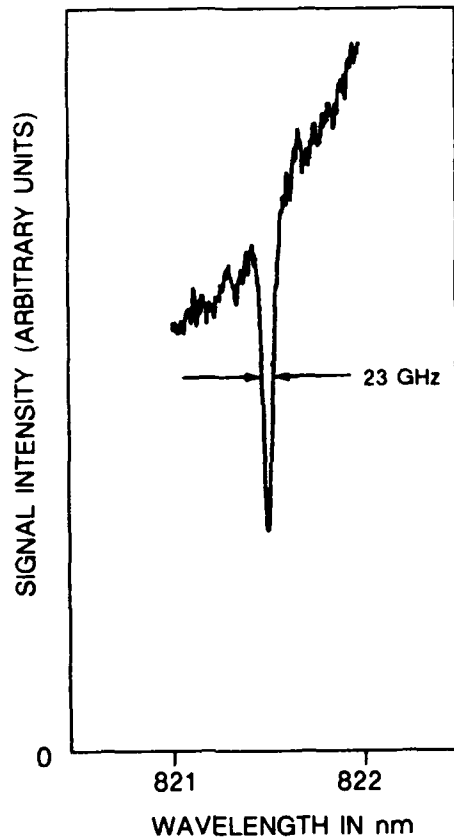


Fig. 2-7. Transmission spectrum of a Bragg grating filter in an optical fiber.

89-6-66-5

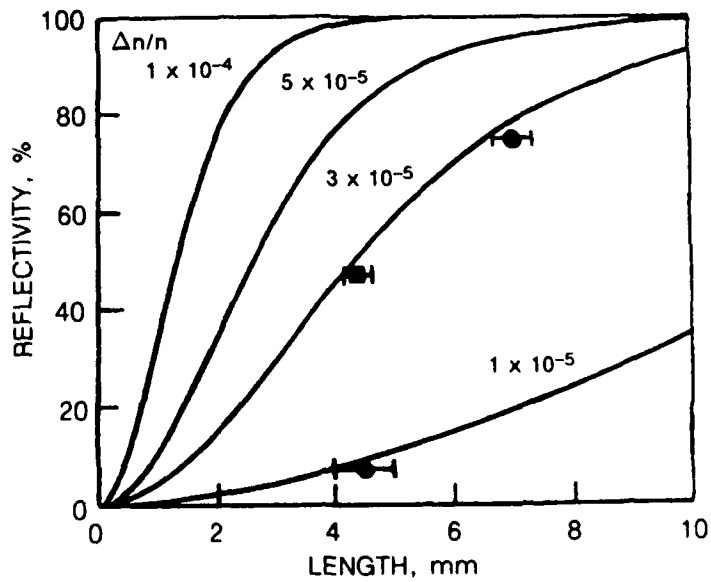


Fig. 2-8. Bragg grating reflectivities for different fractional index changes.

90-1-49-4

Figure 2-9 shows a plot of the grating strength as a function of exposure time. This was measured on a sample of Andrew Corp. elliptical core fiber. The saturation of the index change is evident. Here the exposure intensity was 3.5 watts/cm^2 and the saturation occurred after a few minutes of exposure. The saturation properties vary from fiber to fiber but the exposure conditions shown in the figure are fairly typical.

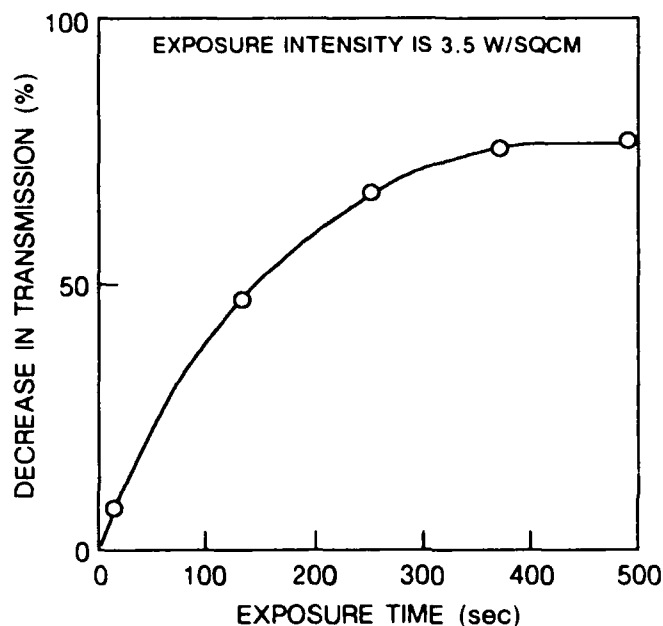


Fig. 2-9. Strength of Bragg grating vs exposure for Andrew fiber.

90-1-49-5

An interesting and useful phenomenon was observed in the investigation of the Bragg gratings. If blue light from an argon laser is propagated in a fiber with an embedded grating, the region where the grating exists emits a red fluorescence. Presumably the bleaching of the UV absorption leads to the formation of another type of center that has an absorption at 457 nm and subsequently decays via the fluorescence. This fluorescence can certainly provide information on the nature of the states involved. Time did not permit a thorough investigation of this phenomenon during the program. Figure 2-10 shows a spectrum of the fluorescent emission. The fluorescence is independent of the grating periodicity. It occurs when a section of the fiber is exposed to a single UV beam. The fluorescence is useful in that it allows the determination of the location of a grating in a section of fiber.

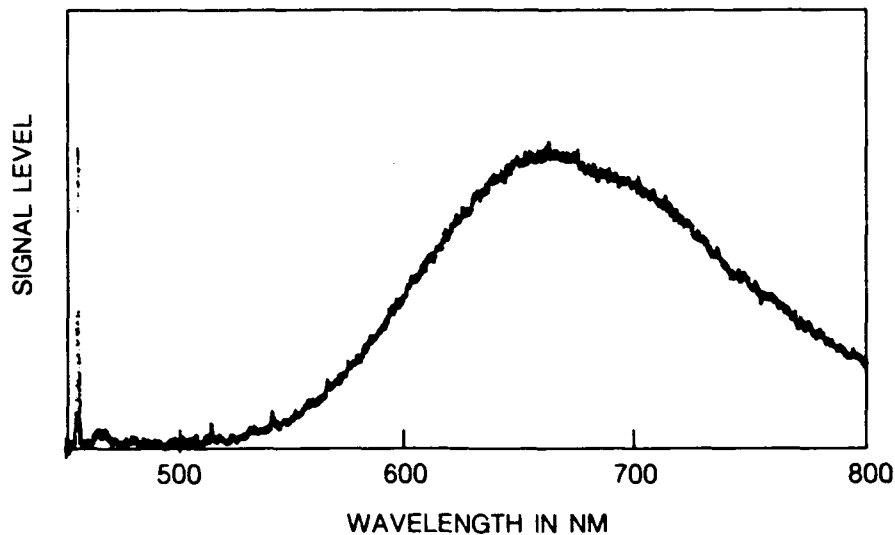


Fig. 2-10. Fluorescence from exposed section of fiber excited by 457.9 NM argon laser line.

90-1-49-6

2.4 MODE AND POLARIZATION DEPENDENCE OF REFLECTIVITY

In a fiber that can support more than one mode, the various transverse modes will have their reflectivity peaks at different values of the free space wavelength. The reflectivity peak occurs when the axial wavenumber of the mode is equal to one-half the grating wavenumber. In the experiments around 580 nm, the fiber was not single mode and could support the next higher mode. A transmission spectrum is shown in Fig. 2-11. The transmission dip at the shorter wavelength corresponds to the second mode. The predicted separation of the peaks was calculated from the dispersion relation for the fiber and was within ten percent of the measured value.

Gratings have been made in polarizing preserving fiber. The effective index of refraction is different for the two states of polarization so that one would expect to see two transmission dips for unpolarized light input, one for each mode. Figure 2-12 shows the transmission for a grating produced in Andrew elliptical core fiber. The unpolarized light shows the two dips as expected. With polarized light, two separate dips were observed. The separation of the dips agrees closely with the value calculated from the known beat length of 4.5 mm. The depths of the two peaks are different. This

results from the fact that the sensitivity of the spectrometer used was different for the two states of polarization.

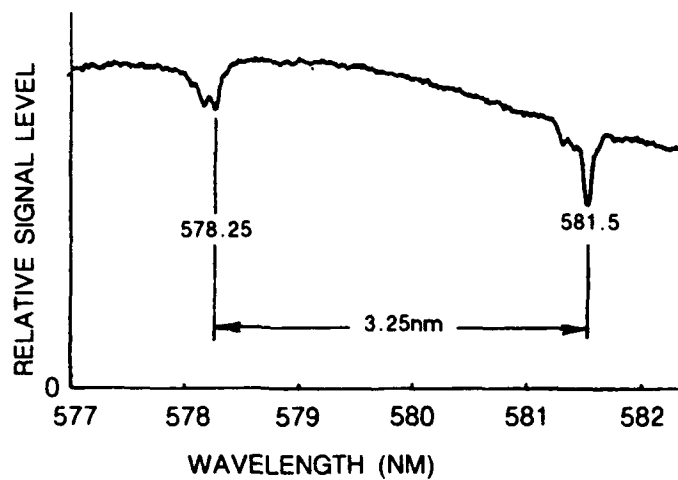


Fig. 2-11. Transmission dip due to higher order transverse mode.

89-6-66-7

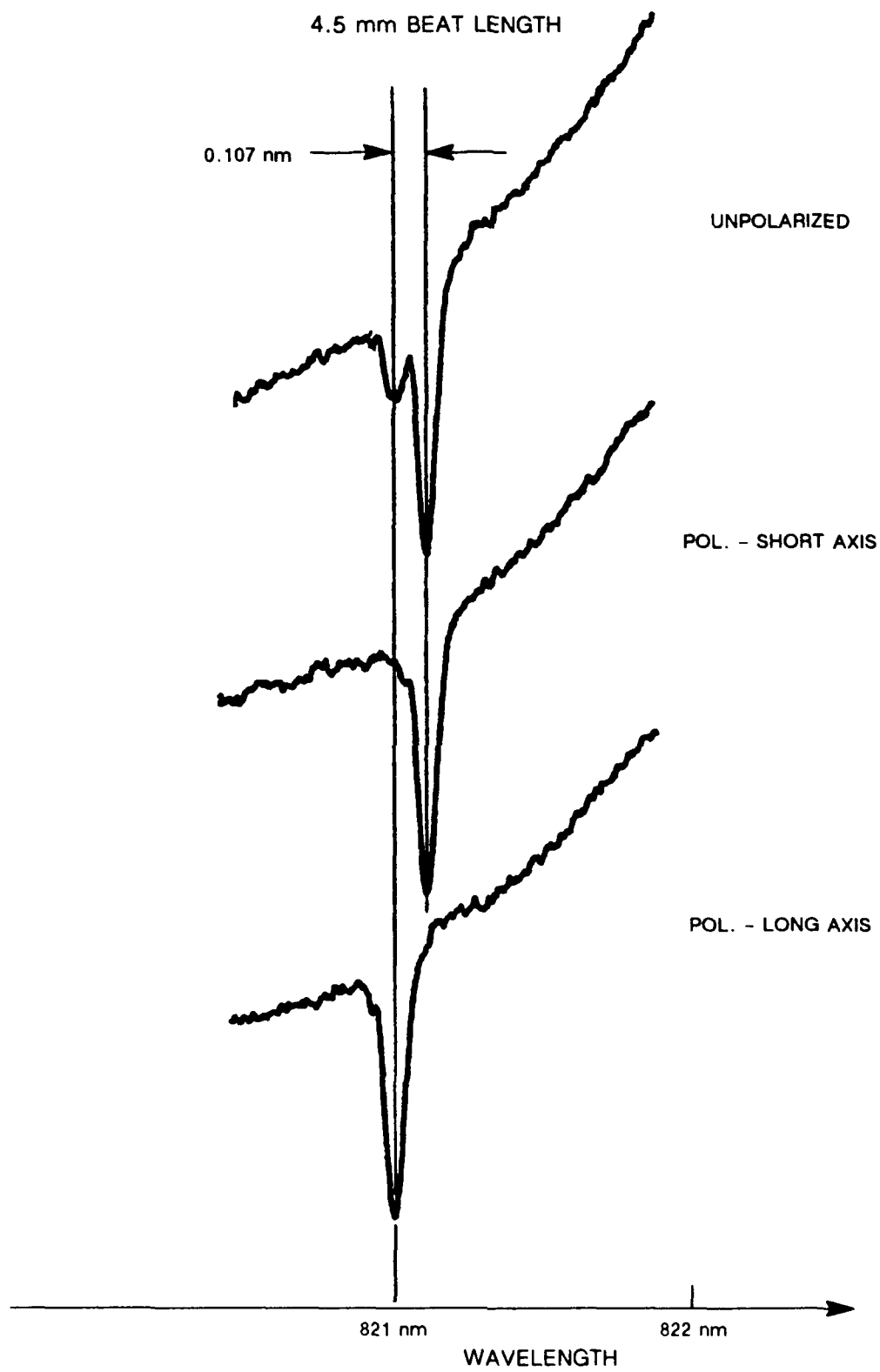


Fig. 2-12. Bragg grating in elliptical fiber.

89-6-66-6

2.5 TEMPERATURE AND STRAIN SENSITIVITY

If a fiber with an embedded grating is heated, the refractive index and the dimensions of the fiber will change and the wavelength of peak reflectivity will shift. The shift is given by

$$\delta\lambda/\lambda = (\alpha + \zeta)\Delta T$$

where

α = expansion coefficient for the fiber

$$= .55 \times 10^{-6} \text{ }^{\circ}\text{C}^{-1}$$

ζ = thermooptic coefficient

$$= 8.31 \times 10^{-6} \text{ }^{\circ}\text{C}^{-1}$$

$$\delta\lambda/\lambda = 8.86 \times 10^{-6} \Delta T$$

Figure 2-13 shows the measured shift in the location of the reflectivity peak of a fiber grating up

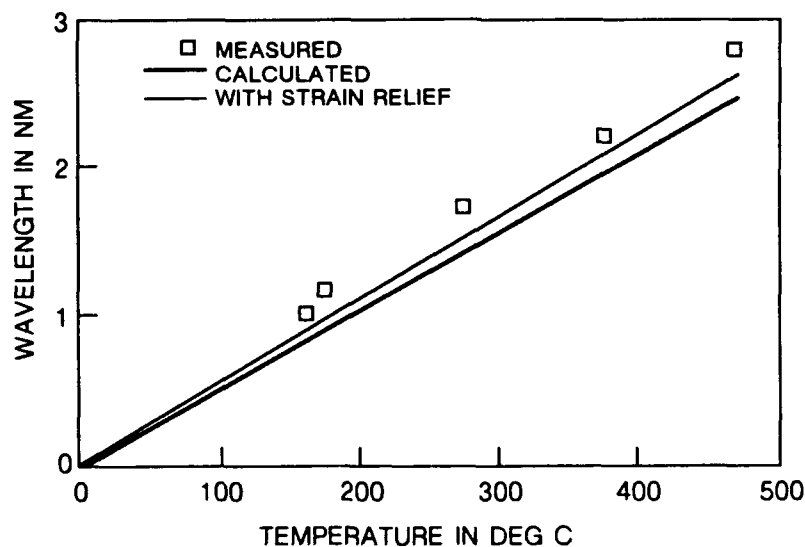


Fig. 2-13. Shift in Bragg wavelength with temperature change.

90-1-49-7

to a temperature of 500 °C. The shift is quite linear and in good agreement with the calculated response. It is significant that the grating persisted at the elevated temperature. When the fiber was allowed to cool, the peak shifted back reversibly to its original location. In a later experiment, a grating

was heated to between 500 °C and 800 °C. In this case, there was an irreversible change in the grating; the lineshape was changed and upon cooling, did not return to its original condition. This is the region in which the fiber begins to soften so such changes would be expected.

Similarly, if a fiber is strained, its index and the periodicity of the grating will change leading to a shift in the peak. This may be calculated to be

$$\delta\lambda/\lambda = (1 - p_e) \epsilon$$

where

p_e = photoelastic constant

ϵ = $\delta L/L = Y^{-1} F/A$; Y = Young's modulus = 1.04×10^7 psi

F/A = Force/unit area

$\delta\lambda/\lambda = 7.50 \times 10^{-8} F/A$

Figure 2-14 shows the measured shift in the reflectivity peak as a function of applied stress, together with the calculated values. Again, the agreement is quite good.

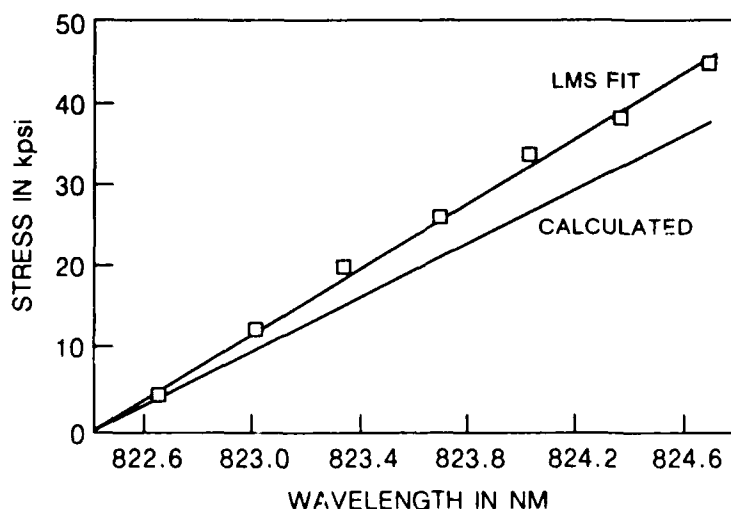


Fig. 2-14. Shift in Bragg wavelength with applied stress.

90-1-49-8

2.6 COUPLING OF RADIATION OUT OF A FIBER BY A GRATING

All of the previous discussions and experimental results have been concerned with the case in which the phase fronts of the embedded grating were perpendicular to the fiber axis. We now consider the case of tilted gratings. In general, the radiation scattered by an embedded grating will be a maximum for the wavelength and direction that satisfy the Bragg condition. The Bragg condition is the condition that satisfies both energy and momentum conservation. For a perpendicular grating, the situation is as shown in Fig. 2-15a. Energy conservation requires that the frequency of the incident

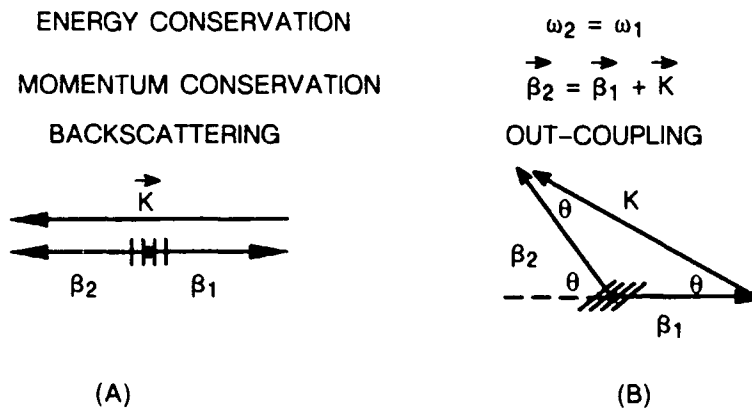


Fig. 2-15. Bragg conditions.

90-1-49-14

radiation and the scattered radiation be the same. Momentum conservation requires that the incident wavevector, $\vec{\beta}_1$, plus the wavevector of the grating, \vec{K} , equal the wavevector of the scattered radiation, $\vec{\beta}_2$. For perpendicular grating, all the wavevectors are collinear. The scattered wavevector is equal in magnitude and opposite in sign to the incident wavevector so that the momentum conservation condition gives

$$2\beta = K$$

$$\frac{\lambda}{n} = 2\Lambda_g$$

This is the Bragg condition discussed previously. The case of a tilted grating is shown in Fig. 2-15b. Here the wavevector of the grating is inclined at an angle, θ_g , with respect to the fiber axis. The magnitudes of the incident and scattered wavevectors must be the same. Elementary trigonometry shows that the scattered wavevector must be at an angle $2\theta_g$ with respect to the fiber axis. Applying the law of cosines to the momentum diagram gives

$$|\beta_1|^2 + |\beta_2|^2 - 2 |\beta| |\beta_2| \cos (180 - 2\theta_g) = |K|^2$$

$$2\beta^2 (1 + \cos 2\theta_g) = K^2$$

$$4\beta^2 \cos^2 \theta_g = K^2$$

$$2\beta \cos \theta_g = K$$

This analysis strictly applies to infinite plane waves. In this case, there is only one angle and one wavelength that is scattered efficiently. In the case of the embedded grating, there is a considerable spread in the grating wavevector in the direction transverse to the fiber core. We can treat this by considering the separate vector components of the momentum matching condition. We now allow the radiation to be scattered at some angle θ that is different from $2\theta_g$. For the transverse component

$$\beta \sin \theta = K \sin \theta_g + \Delta K$$

Here ΔK is the spread in the transverse component due to the small core diameter. This spread allows the equation to be satisfied for a range of values of the scattering angle. The longitudinal component gives

$$-\beta \cos \theta = \beta - K \cos \theta_g$$

$$\beta (1 + \cos \theta) = K \cos \theta_g$$

$$\cos \theta = \frac{K}{\beta} - K \cos \theta_g - 1$$

This determines the scattering angle as a function of the incident wavelength. The embedded grating can thus act as a spectrometer, coupling out different wavelengths at different angles.

An experiment was carried out to investigate the coupling of radiation out of a fiber. A 5 mm long grating was made in an elliptical core, D-shaped, polarization maintaining fiber. The fiber was rotated to form Bragg planes at approximately 40° with respect to the major axis of the elliptical core and normal to the flat face of the fiber. Figure 2-16 shows the coupling of HeNe radiation out of the fiber. This figure is a double exposure. One exposure was taken with the camera focused on the fiber. The second exposure was then taken with the camera focused at infinity to obtain the far field pattern. At the 633 nm wavelength, the fiber could support two modes in each of the orthogonal polarization states. As a result, two pairs of beams are radiated. Each of the beams seen in the figure is actually a pair of beams, one for each state of polarization. Figure 2-17 shows a trace of the far field intensity of this pattern. The scattering angle is measured with respect to the direction normal to the fiber. A polarizer was used to separate the two polarization components. The perpendicular polarization is the one perpendicular to the fiber's major axis. The parallel polarization is the one orthogonal to the perpendicular polarization and the direction of propagation. Since the radiation is being scattered nearly normal to the fiber. The dipole factor greatly reduces the intensity of the parallel component. The scattered intensity at 633 nm was approximately 3×10^{-4} of the incident intensity. Experiments were also carried out at other wavelengths. These verified the angle vs wavelength dependence of the scattering. A scattering efficiency of 2×10^{-3} was measured at 514 nm.

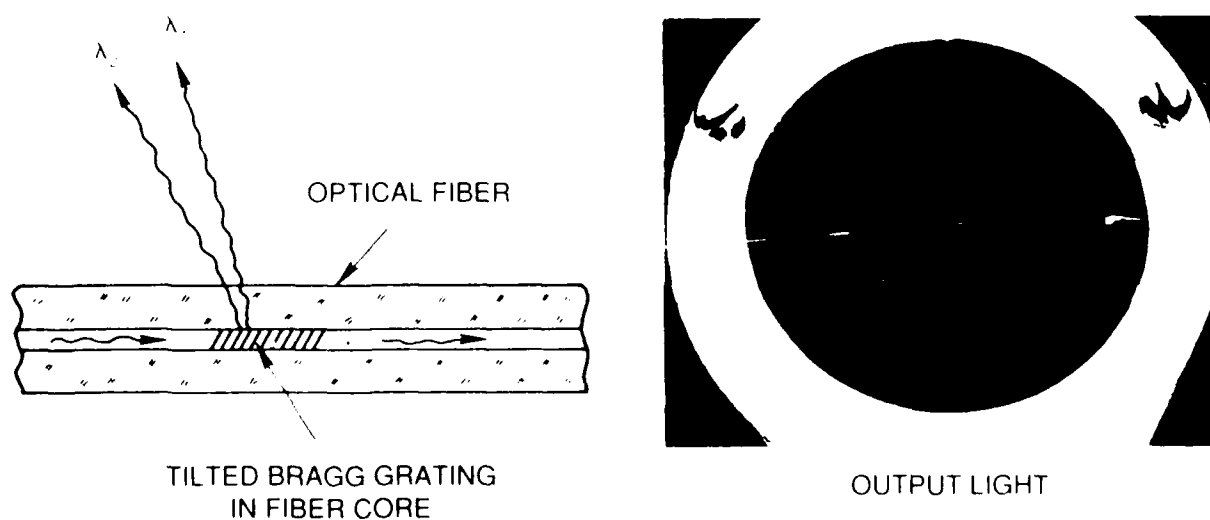


Figure 2.16 Wavelength-selective light coupling from fibers with bragg coatings.

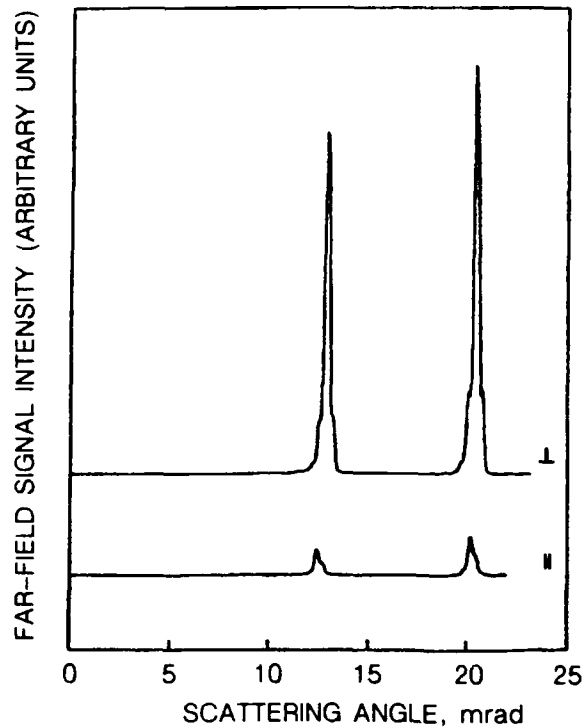


Fig. 2-17. Outcoupling of light by a grating.

90-1-49-13

2.7 LOCKING AND TUNING OF AN EXTERNAL CAVITY SEMICONDUCTOR LASER WITH AN EMBEDDED FIBER GRATING REFLECTOR

Since an embedded grating is a narrowband reflector, it may be used as a reflector in an external cavity laser to lock the frequency of the laser to the reflectivity peak. The frequency may then be tuned by strain or temperature as discussed above.

A grating was produced with a 58% reflectivity in a bandwidth of 0.05 nm around 822 nm. A 32 cm length of fiber terminated by this grating was butt coupled to the output facet of a commercial gain-guided AlGaAs diode laser having 90% and 3% reflectivity at the rear facet and the output facet, respectively. Due to inefficiency in the fiber to laser coupling, the grating-to-laser feedback was not more than a few percent.

With the external feedback fully disabled, by misalignment of the fiber-to-laser coupling, the laser usually operated on several modes of the optical cavity formed by the laser chip facets, as shown in Fig. 2-19a. Brief periods of single mode operation were achieved by carefully adjusting the drive current. The nominal output wavelength was near 816 nm and the single-mode linewidth was about 50

MHz. With the coupling aligned, and with the laser temperature and drive current adjusted to place a chip mode within the grating bandwidth, the laser output shifted to the 822 nm grating wavelength as illustrated in Fig. 2-17b.

Fabry-Perot interferometry showed that within a single chip-cavity mode, several external-cavity modes spaced by about 320 MHz (corresponding to the 47 cm effective optical length) often oscillated simultaneously as shown in Fig. 2-18a. With the fiber-to-chip coupling carefully aligned, all but one of these modes could be substantially quenched, as shown in Fig. 2-18b. A delayed self heterodyne measurement showed the linewidth of the remaining mode to be as small as 200 KHz.

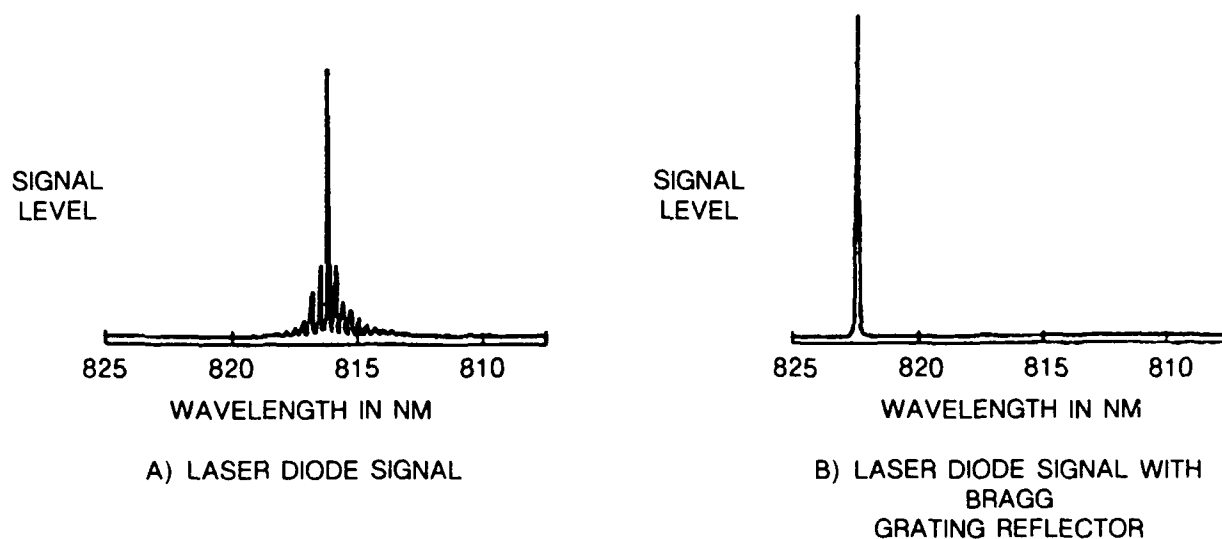
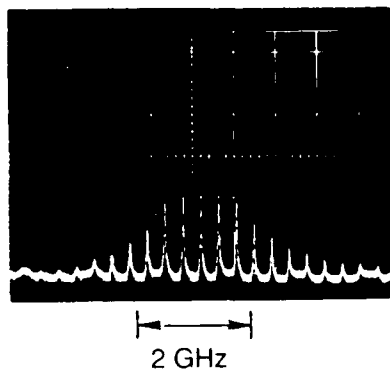


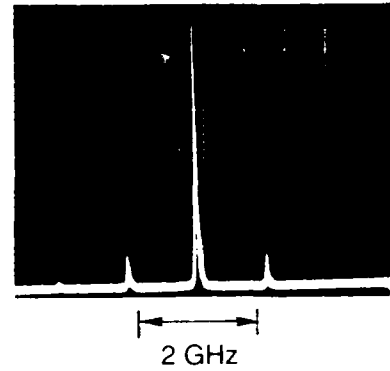
Fig. 2-18. Controlling the emission of a laser diode with the reflection from a Bragg grating in an optical fiber.

90-1-49-11

The external feedback was strong enough to support laser oscillation only when the grating wavelength matched that of a chip mode. When the grating period was varied, either by applying axial stress or by controlling the temperature, the laser output wavelength tuned discontinuously from one chip mode to the next. Stress tuning over a 2 nm wavelength range, corresponding to seven axial modes of the chip, was easily achieved in preliminary tests. The stress response data, shown in Fig. 2-19, were actually obtained by monitoring the output wavelength of the external cavity laser. Continuous tuning over this range can be anticipated if the external feedback coupling is improved and the chip output facet reflectivity is reduced.



a) BEFORE FINE ADJUSTMENT



b) AFTER FINE ADJUSTMENT

Figure 2-19 Single grating-selected laser-chip mode (scanning Fabry-Perot display).

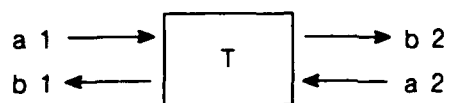
Fig. 2-19. Single grating-selected laser-chip mode (scanning Fabry-Perot display).

90-1-49-12

2.8 MULTIPLE GRATING CONFIGURATIONS

It is of interest to consider fiber structures involving two or more gratings separated by regions of unperturbed fiber. This situation may be analyzed readily using the T matrix formalism [4]. The basis of this approach is shown in Fig. 2-20. The section of fiber with the grating is treated as a four port element with inputs a_1 and a_2 from either side and outputs b_1 and b_2 . The relations between the inputs and the outputs are determined by the complex reflection and transmission coefficients. These are given in [3] for a grating of arbitrary length, strength and center frequency. The expressions are somewhat cumbersome and will not be reproduced here. The input-output relations may be recast in the form shown in the figure. The T matrix relates the input and output on the right side of the element to the corresponding quantities on the left side. The T matrix for a section of unperturbed fiber is also easily derived. The beauty of the T matrix is illustrated in Fig. 2-21. The T matrix for cascaded elements is simply the matrix product of the T matrices of the individual elements. With this approach, complex structures involving identical or different gratings separated by arbitrary spaces may readily

be analyzed. Commercially available software packages such as MATHCAD are well suited to this type of calculation.



$$\begin{aligned} a_2 &= T_{aa} a_1 + T_{ab} b_1 \\ b_2 &= T_{ba} a_1 + T_{bb} b_1 \end{aligned}$$

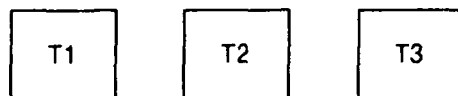
FOR A MIRROR

$$T = \begin{array}{|c|c|} \hline r/jt & 1/jt \\ \hline -1/jt & r/jt \\ \hline \end{array}$$

Fig. 2-20. T matrix.

90-1-49-15

FOR CASCADED ELEMENTS



IS EQUIVALENT TO
 $T = T_3 \times T_2 \times T_1$

Fig. 2-21. Beauty of the T matrix.

90-1-49-16

Figure 2-22 shows a simple example of the results. The structure is a fiber Fabry-Perot resonator consisting of two identical gratings of one centimeter length separated by a space of two centimeters. The reflectivity of each grating was 80%. Within the transmission dip of the individual grating response, there are transmission bands corresponding to the Fabry-Perot resonances of the structure. These bands can become extremely narrow for large spacing of the gratings.

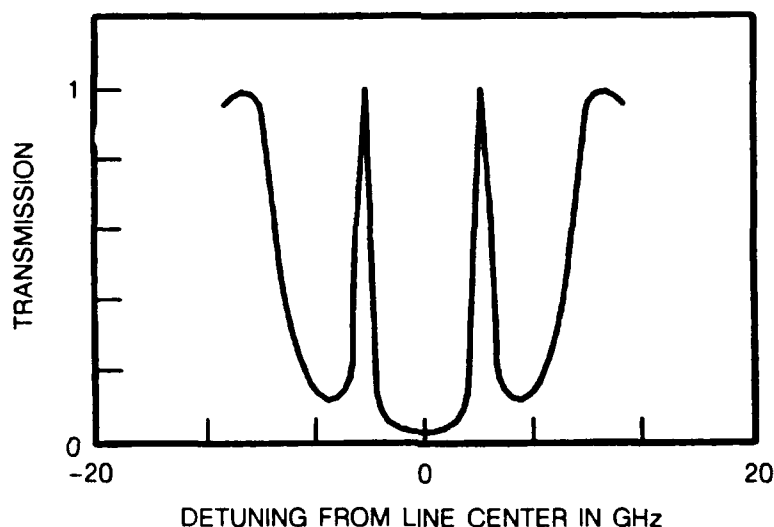


Fig. 2-22. Calculated spectrum of Fabry-Perot resonator formed with bragg gratings.

90-1-49-17

3.0 CONCLUSIONS

Work on this program has demonstrated that strong, localized Bragg reflectors may be readily formed in fibers by exploiting the photorefractive effect in germanosilicate glasses. Previously, gratings have been formed in fibers by polishing away the fiber cladding and producing periodic perturbations by photolithographic techniques. This is a rather elaborate, time-consuming and expensive procedure. The present technique is extremely convenient and simple. Gratings can be produced in a matter of minutes with minimal disturbance to the fiber. This offers great promise for the practical realization of a wide variety of optical devices for sensor and signal processing applications.

Sensors for temperature, strain or other parameters may be made based on the change in the grating period and index in response to environmental changes. Coatings may be applied to the fiber to allow sensing of electric and magnetic fields. Directionally sensitive sensors may be made using gratings in birefringent fibers. Alternatively, the gratings may be used simply as controllable narrowband reflectors and measurements may be made of the change in optical path length of sections of fiber between reflectors. Multiplexed, distributed sensors may be made using a variety of wavelength, time domain, frequency domain and coherence multiplexing schemes. One can even envision a phased array of sensors on a single optical fiber.

A wide variety of optical signal conditioning components based on embedded gratings is possible. Extremely narrow bandpass and band stop filters can be made. Filters with complex transmission characteristics may be synthesized. Tapped delay lines, transversal filters and optical matched filters may be realized. These can operate on the optical signal itself or on a microwave modulation imposed on the optical carrier. Rapidly programmable transversal filters are also possible. Sets of gratings with different tap weights can be formed at different wavelengths and the desired set of tap weights may be selected by changing the wavelength of the optical carrier. Wavelength selective taps have been demonstrated and should be useful in wavelength multiplexed systems. Filters may be made to affect the different transverse modes selectively in a multimode fiber. The use of an embedded grating to lock and tune the frequency of an external cavity semiconductor laser has been demonstrated. With appropriate temperature control it may be possible to use the

gratings as optical frequency standards in a way analogous to quartz crystals at lower frequencies. It should also be possible to make an all fiber grating-tuned laser using a germanosilicate fiber with a rare earth dopant and a semiconductor diode laser pump.

Much work remains to be done to elucidate the details of the photorefractive process and to optimize the photosensitivity. It is known that the formation of the photosensitive centers is favored by processing the glass at high temperature and subsequently allowing rapid cooling. This thermal cycle could occur during the formation of the preform or in the actual drawing of the fiber. Variations in sensitivity are observed in nominally similar samples of commercial fiber, presumably due to slight variations in the processing history of the fiber. Gratings have been formed successfully, however, in a variety of different commercially available fibers so that the practical realization of optical components based on embedded gratings need not await the thorough understanding of the photorefractive process itself.

4.0 REFERENCES

1. K. O. Hill, Y. Fujii, D. C. Johnson and B. S. Kawasaki, Appl. Phys. Lett., 32, 647 (1978).
2. J. M. Jackson, M. E. Wells, G. Kordas, D. L. Kinser and R. A. Weeks, J. Appl. Phys., 58, 2308 (1985).
3. D. K. W. Lam and B. K. Garside, Appl. Optics, 20, 440 (1981)
4. H. H. Haus, Waves and Fields in Optoelectronics, Prentice-Hall, Inc., Englewood Cliffs, NH (1984).

5.0 PUBLICATIONS AND PRESENTATIONS

The following is a list of publications and presentations on work supported in part by Contract F19628-88-C-0033.

G. Meltz, W. W. Morey and W. H. Glenn, "In-Fiber Bragg Grating Tap," Presented at the OFC '90 Conference on Optical Fiber Communication, San Francisco, CA, January 22-26, 1990.

W. W. Morey, G. Meltz and C. M. Ferrar, "Tunable Narrowband External-Cavity Diode Laser With a Fiber Grating Reflector," Presented at the OFC '90 Conference on Optical Fiber Communication, San Francisco, CA, January 22-26, 1990.

W. W. Morey, G. Meltz and W. H. Glenn, "Bragg Gratings in Optical Fibers," to be presented at the Department of Defence Fiber Optics Conference '90, McLean, VA, March 20-23, 1990.

G. Meltz, J. R. Dunphy and W. W. Morey, "Fiber-Optic Bragg-Grating Sensors for Smart Structures," to be presented at the Instrument Soc. of America Annual Meeting, New Orleans, LA, October 14-18, 1990.

W. W. Morey, "Bragg Gratings in Optical Fibers," presented at a seminar at Rutgers University, February 23, 1989. G. Meltz, W. W. Morey and W. H. Glenn, "Formation of Bragg Gratings in Optical Fibers by a Transverse Holographic Method," Published in Optics Letters, Vol. 14, No. 15, August 1, 1989.

W. W. Morey, G. Meltz and W. H. Glenn, "Fiber Optic Bragg Grating Sensors," Presented at OE/Fibers '89, SPIE Conference, Boston, MA, September 5-8, 1989. W. W. Morey, G. Meltz and W. H. Glenn, "Bragg-grating Temperature and Strain Sensors," Presented at the 6th International Conference on Optical Fiber Sensors, Paris, France, September 18-20, 1989.

W. H. Glenn, "Embedded Gratings in Optical Fibers," EECS/RLE Seminar, M.I.T., November 16, 1988.



MISSION of Rome Air Development Center

RADC plans and executes research, development, test and selected acquisition programs in support of Command, Control, Communications and Intelligence (C³I) activities. Technical and engineering support within areas of competence is provided to ESD Program Offices (POs) and other ESD elements to perform effective acquisition of C³I systems. The areas of technical competence include communications, command and control, battle management information processing, surveillance sensors, intelligence data collection and handling, solid state sciences, electromagnetics, and propagation, and electronic reliability/maintainability and compatibility.